The EMBO Journal Vol. 20 No. 21 pp. 5853–5862, 2001

Shedding light on disulfide bond formation: engineering a redox switch in green fluorescent protein

Henrik Østergaard[1,2], Anette Henriksen[3], Flemming G.Hansen[1] and Jakob R.Winther[2,4]

[1]Section of Molecular Microbiology, BioCentrum-DTU, Technical University of Denmark, Building 301, DK-2800 Lyngby and Departments of [2]Physiology and [3]Chemistry, Carlsberg Laboratory, Gamle Carlsberg Vej 10, DK-2500 Copenhagen Valby, Denmark

[4]Corresponding author
e-mail: jrw@crc.dk

To visualize the formation of disulfide bonds in living cells, a pair of redox-active cysteines was introduced into the yellow fluorescent variant of green fluorescent protein. Formation of a disulfide bond between the two cysteines was fully reversible and resulted in a >2-fold decrease in the intrinsic fluorescence. Interconversion between the two redox states could thus be followed *in vitro* as well as *in vivo* by non-invasive fluorimetric measurements. The 1.5 Å crystal structure of the oxidized protein revealed a disulfide bond-induced distortion of the β-barrel, as well as a structural reorganization of residues in the immediate chromophore environment. By combining this information with spectroscopic data, we propose a detailed mechanism accounting for the observed redox state-dependent fluorescence. The redox potential of the cysteine couple was found to be within the physiological range for redox-active cysteines. In the cytoplasm of *Escherichia coli*, the protein was a sensitive probe for the redox changes that occur upon disruption of the thioredoxin reductive pathway.

Keywords: fluorescence indicator/oxidoreductase/redox potential/thioredoxin reductase/YFP

Introduction

While disulfide bonds serve as important structural components of many of the proteins exported from the cell, they are almost completely absent from their cytosolic counterparts (Gilbert, 1990). In the periplasm of *Escherichia coli*, disulfide bonds are introduced into nascent proteins through the action of the DsbA and DsbC pathways (reviewed by Rietsch and Beckwith, 1998; Debarbieux and Beckwith, 1999). In the cytosol, protein disulfide bonds are also found; however, here they are only formed transiently. Thus, disulfides are found as part of the catalytic cycle of enzymes such as ribonucleotide reductase or in redox-regulated proteins such as the chaperone Hsp33 and the transcription factor OxyR (Aberg *et al*., 1989; Zheng *et al*., 1998; Jakob *et al*., 1999). Maintenance of protein sulfhydryls in general as well as recycling of these proteins to the reduced state relies on two partially redundant pathways, one involving thioredoxins (encoded by *trxA* and *trxC*) and the other glutaredoxins (encoded by *grxA*, *B* and *C*) (Prinz *et al*., 1997; Aslund and Beckwith, 1999). These thiol–disulfide oxidoreductases belong to a family of enzymes having in common a pair of redox-active cysteines in a Cys-Xaa-Xaa-Cys motif (Martin, 1995). Cycling of the active site cysteines between the reduced and oxidized state allows them to undergo disulfide exchange reactions with protein substrates or small thiol compounds such as glutathione. Both pathways rely on NADPH as the source of reducing equivalents. In the thioredoxin pathway, they are delivered to thioredoxin by the flavoenzyme thioredoxin reductase (encoded by *trxB*), while electrons are transferred via glutathione reductase and glutathione to the glutaredoxins (Holmgren, 1989).

Characterization of the pathways leading to the formation or reduction of disulfide bonds has relied extensively on the use of naturally occurring proteins as endogenous probes of the cellular thiol–disulfide redox state. These have been selected based on discernible characteristics of their oxidized and reduced state such as enzymatic activity [e.g. alkaline phosphatase (Derman *et al*., 1993) and β-galactosidase (Bardwell *et al*., 1991; Jonda *et al*., 1999)] and electrophoretic mobility (e.g. OmpA and β-lactamase; Bardwell *et al*., 1991). However, although a variety of such reporters are available in *E.coli*, only few exist in yeast and mammalian cells and none support non-invasive redox monitoring at the single-cell level. To overcome these limitations, we have engineered a new type of redox reporter based on the fluorescent properties of green fluorescent protein (GFP). Besides its bright and visible fluorescence, GFP exhibits a number of attractive features for *in vivo* reporter applications. It is chemically inert and does not interfere with cellular processes; contains no disulfide bonds, and can be targeted specifically to subcellular compartments such as the endoplasmic reticulum, mitochondria and the periplasmic space in bacteria (De Giorgi *et al*., 1999; Casey *et al*., 2000).

GFP consists of 238 amino acids folded into an 11-stranded β-barrel wrapped around a central irregular α-helix (see Figure 1A) (Ormo *et al*., 1996; Yang *et al*., 1996). The chromophore is situated in the middle of the α-helix and is generated by an autocatalytic cyclization of the tripeptide segment -Ser65-Tyr66-Gly67- (Cody *et al*., 1993; Heim *et al*., 1994; Reid and Flynn, 1997). Mutagenesis of the chromophore sequence and the surrounding barrel structure has resulted in variants with significantly altered absorption and emission spectra (reviewed by Tsien, 1998; Palm and Wlodawer, 1999; Remington, 2000). One example is the yellow fluorescent variant of GFP (YFP) with a Thr→Tyr mutation at position 203. In the crystal structure of YFP (termed wtYFP in the following), the highly polarizable tyrosine side chain stacks with the phenolic moiety of chromo-

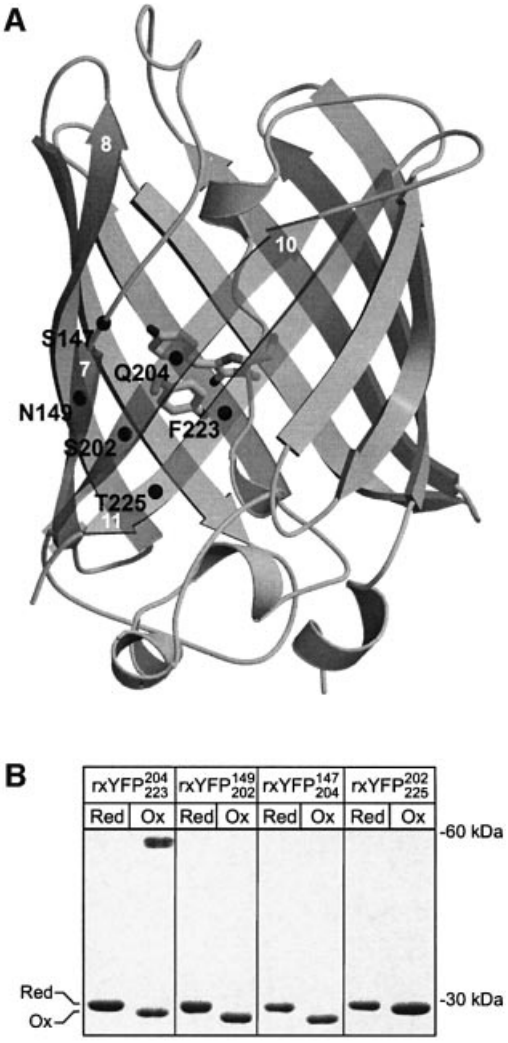

Fig. 1. Cysteine mutants of the yellow fluorescent protein. (**A**) The six positions at which cysteines residues were introduced are marked with black spheres in the crystal structure of wtYFP (Wachter *et al*., 1998). The chromophore and the side chain of Tyr203 are shown as stick representations. Relevant β-strands are numbered in white according to Yang *et al*. (1996). (**B**) Spontaneous oxidation of the cysteine mutants as monitored by non-reducing SDS–PAGE. Reduction of the four mutant proteins was performed by overnight incubation with 20 mM DTT. Subsequently they were dialysed against 20 mM Tris–HCl pH 8.0 for 17 h at room temperature to promote oxidation. Trichloroacetic acid (10% v/v) was added to aliquots of the samples taken before (marked Red) and after (marked Ox) dialysis. The protein precipitate was washed twice with acetone and then alkylated with 50 mM *N*-ethylmaleimide before analysis by non-reducing SDS–PAGE on a 16% gel.

phore, leading to a red shift of the fluorescence spectrum (Wachter *et al*., 1998).

Using YFP as a template, we present here the design and the biochemical and structural characterization of a novel fluorescent disulfide bond reporter and show that it is a sensitive probe of the redox state in the cytoplasm of *E.coli*.

Results

Engineering disulfide bonds in YFP

The spectral properties of GFPs are determined in part by a number of non-covalent interactions between the chromophore and residues in the surrounding barrel structure. The majority of these residues are situated on the inner side of three consecutive β-strands 7, 10 and 11, shielding the chromophore from the bulk solvent (Figure 1A). In wtYFP, these residues constitute His148, Tyr203, Glu222, Asn146 and Ser205 (Wachter *et al*., 1998). Previous studies have identified this region of the β-barrel as being structurally flexible, tolerating the introduction of new N- and C-termini by circular permutation and even insertion of entire protein domains (Baird *et al*., 1999; Topell *et al*., 1999). This led us to speculate that reversible formation of a strained disulfide in this part of the protein might perturb the surrounding structure sufficiently to bring about a measurable change in the fluorescent properties of the protein. By visual inspection of the crystal structure of wtYFP, four pairs of residues 147–204, 149–202, 202–225 and 204–223, were found suitable for disulfide engineering. As shown in Figure 1A, each pair bridges two of the three β-strands interacting with the chromophore and are, furthermore, solvent exposed to enable free access of the surrounding redox buffer.

GFP contains two native cysteines, Cys48 and Cys70. Previous work by Inouye and Tsuji (1994) indicated that Cys48, being partially solvent exposed, might be susceptible to modification by thiol-specific reagents. To avoid interfering side reactions, it was substituted for a valine (see Materials and methods for details). The four proteins were produced in high yield in *E.coli*, indicating that the mutations did not significantly impair protein folding or autocatalytic formation of the chromophore. In the following, they will be referred to as rxYFP$^{Xaa1}_{Xaa2}$, where Xaa1 and Xaa2 designate the two positions at which cysteines were introduced.

To investigate whether the four cysteine variants were able to form disulfide bonds under oxidizing conditions, the purified proteins were dialysed against air-saturated buffer at pH 8.0. Pre-treatment with dithiothreitol (DTT) was performed to reduce any disulfide bonds present in the starting material. For each of the proteins, complete oxidation was found to occur within hours, observed by non-reducing SDS–PAGE as a slight increase in electrophoretic mobility (Figure 1B). One of the mutant forms, rxYFP$^{204}_{223}$, in addition to forming oxidized monomers, also associated into disulfide-bonded dimers (apparent as a band at ~60 kDa). These were highly stable and required prolonged incubation with high concentrations of DTT to dissociate (data not shown). Consequently, rxYFP$^{204}_{223}$ was not investigated further.

The most pronounced difference in the fluorescent properties of the reduced and oxidized state was observed for rxYFP$^{149}_{202}$, where formation of the disulfide resulted in a 2.2-fold reduction of the emission peak at pH 7.0 (Figure 2). In comparison, rxYFP$^{147}_{204}$ and rxYFP$^{202}_{225}$ only displayed an ~1.2-fold change. Apart from the change in amplitude, the spectra of the two redox states were essentially identical and similar to those of wtYFP, with excitation and emission peaks at 512 and 523 nm, respectively, and a minor shoulder around 488 nm. The substantial spectral response of rxYFP$^{149}_{202}$ to changes in its redox state prompted us to characterize this variant in further detail.

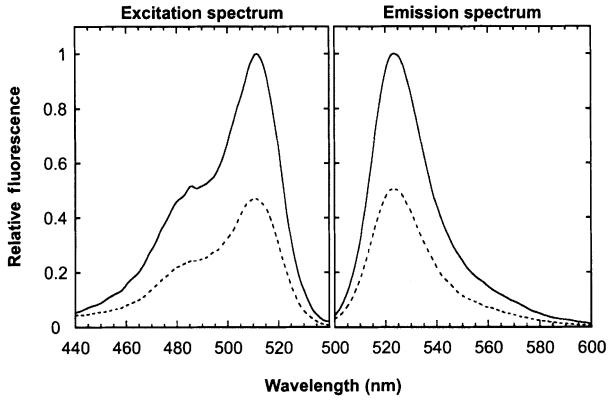

Fig. 2. Fluorescence excitation and emission spectra of oxidized (dashed line) and reduced (solid line) rxYFP$^{149}_{202}$ in 100 mM potassium phosphate pH 7.0, 1 mM EDTA at 30°C. The two spectra were recorded at emission and excitation wavelengths of 540 and 490 nm, respectively. The fluorescent properties of reduced rxYFP$^{149}_{202}$ are identical to those of the template YFP used (see Materials and methods).

Stability and reactivity of the C149–C202 disulfide bond

The redox potential of the cysteine couple in rxYFP$^{149}_{202}$ was determined from the equilibrium constant of the reaction with glutathione at pH 7.0 and 30°C. By measuring the intrinsic fluorescence of rxYFP$^{149}_{202}$ equilibrated in buffers with various ratios of reduced and oxidized glutathione (abbreviated GSH and GSSG, respectively), K_{ox} was determined to 5.0 ± 0.15 M (Figure 3A). Analysis of the equilibrium mixtures by non-reducing SDS–PAGE (Figure 3A, inset) yielded the same value of K_{ox} and thereby reconfirmed the tight correlation between the intrinsic fluorescence of the protein and its redox state. For the calculation of K_{ox}, it was assumed that the concentration of protein–glutathione mixed disulfide at equilibrium was insignificant, an assumption that was justified by the close fit of the model to the experimental data as well as the high effective molarity of the cysteine residues relative to the concentrations of glutathione used (the equilibrium constant for protein–glutathione mixed disulfides are generally <1) (Gilbert, 1990, 1995). A standard redox potential ($E^{o\prime}$) of –261 mV was calculated from the Nernst equation using an $E^{o\prime}$ value of –240 mV for the GSH/GSSG redox couple (Rost and Rapoport, 1964). In comparison, disulfide redox potentials encountered in proteins vary from –122 mV (DsbA; Wunderlich and Glockshuber, 1993; Huber-Wunderlich and Glockshuber, 1998) to –270 mV (thioredoxin; Lin and Kim, 1989; Krause *et al.*, 1991) for the family of thiol–disulfide oxidoreductases. For disulfide bonds serving structural purposes, it can be as low as –470 mV (Gilbert, 1990).

The reactivity of the disulfide bond was determined from the kinetics of its reaction with DTT at pH 7.0 and 30°C. The time course of the reaction was followed by the increase in fluorescence at 523 nm. Initial experiments made it clear that high concentrations of DTT were required to achieve a reasonable rate of reduction. Therefore, reactions were performed under pseudo first-order conditions with a >10^4 molar excess of DTT (Figure 3B). From a fit of the progress curves to a single exponential function, the apparent second-order rate constant (k_2) was estimated to 24.8 ± 0.6 M/min, which is close to the value of 14.1 M/min reported for reduction of oxidized glutathione by DTT (Szajewski and Whitesides, 1980).

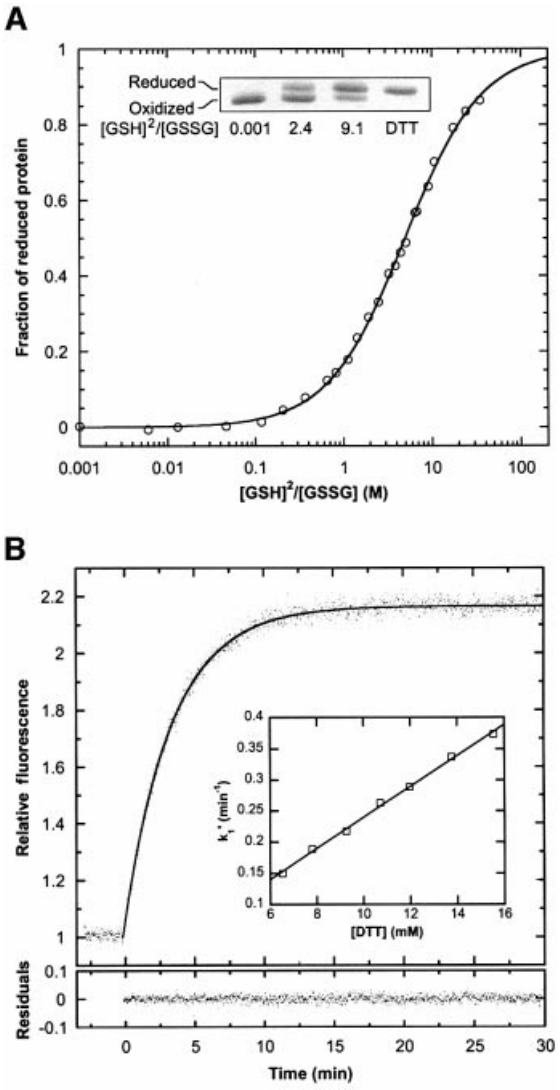

Fig. 3. Stability and reactivity of the disulfide bond in rxYFP$^{149}_{202}$ at pH 7.0 and 30°C. (**A**) Redox titration of rxYFP$^{149}_{202}$ with reduced and oxidized glutathione. After equilibration in buffers with varying [GSH]^2/[GSSG] ratios, the fraction of protein in the reduced state was measured by the intrinsic fluorescence at 523 nm, as described in Materials and methods. Due to trace impurities of GSSG in the commercially available GSH, the last part of the titration curve could not be obtained. However, addition of DTT to a subset of the samples yielded, within experimental error, the same specific fluorescence of the reduced form as was estimated by curve fitting. Inset: the distribution of rxYFP$^{149}_{202}$ between the two redox states as monitored by non-reducing SDS–PAGE. Samples were prepared as described in Figure 1B. (**B**) Reduction of the protein (~0.3 μM) was performed under pseudo first-order conditions with 12 mM DTT in 100 mM potassium phosphate pH 7.0 and 1 mM EDTA. The reaction was followed by the change in fluorescence at 523 nm. A pseudo first-order rate constant (k_1') was obtained by fitting the progress curve to a single exponential function (residuals are shown below the curve). Inset: a plot of k_1' versus [DTT], obtained from a series of similar experiments, yielded a value of 24.8 ± 0.6 M/min for the apparent second-order rate constant.

Spectral properties of rxYFP$^{149}_{202}$

Next, we investigated the mechanism underlying the redox state-dependent shift in fluorescence emission. Figure 4A shows the absorption spectra of the protein at five different points on the redox titration curve given in Figure 3A. Peaks are observed at 404 and 512 nm. Previous studies have shown the two absorption bands to arise from a protonated and deprotonated state of the chromophore, respectively (Chattoraj *et al.*, 1996; Niwa *et al.*, 1996; Brejc *et al.*, 1997; Elsliger *et al.*, 1999). The phenolic moiety of Tyr66 is responsible for this behaviour (Elsliger *et al.*, 1999); it is a weak monoprotic acid and, despite its location in the interior of the β-barrel, it responds rapidly to changes in the external pH. In YFP, the protonated chromophore is non-fluorescent. The increase in the 404/512 nm peak ratio upon oxidation suggests that bridging of the two cysteines shifts the equilibrium between the two chromophore protonation states towards the non-fluorescent, protonated form. This was confirmed by fluorescence pH titrations of the free and disulfide-bonded protein yielding apparent chromophore pK_a values of 6.05 ± 0.01 [Hill coefficient (n) = 1.00] and 6.76 ± 0.01 (n = 0.86), respectively (Figure 4B). Similar values, 6.00 ± 0.01 (n = 0.98) and 6.70 ± 0.03 (n = 0.79), were obtained by absorbance measurements. A shift in the chromophore ionization constant of 0.7 units alone, however, is not sufficient to account for the observed change in the intrinsic fluorescence. Disulfide bond formation also leads to an ~1.5-fold reduction in the molar extinction coefficient of the deprotonated chromophore, which is evident from the lack of convergence of the two absorption pH titration curves at high pH, where the chromophore is predominantly negatively charged (see Figure 4B).

Crystallographic analysis of oxidized rxYFP$^{149}_{202}$

To define the structural basis of the redox state-dependent fluorescence, the crystal structure of oxidized rxYFP$^{149}_{202}$ was determined. The protein was crystallized at pH 8.0 to ensure a homogenous population of deprotonated chromophores. Using wtYFP as a search model, the structure was solved by molecular replacement. The final resolution was 1.5 Å, with R-factors of 18.3 and (R_{free}) 21.2%, respectively (data collection and refinement statistics are given in Table I).

Overall, the crystal structure of rxYFP$^{149}_{202}$ resembles that of wtYFP, with a root mean square deviation of 0.5 Å for the α carbons (Figure 5A). As shown in Figure 5B, significant $2F_o - F_c$ electron density is visible between β-strands 7 (residues 147–153) and 10 (residues 199–208) corresponding to the disulfide bridge, which is completely exposed on the surface of the protein. The cysteine side chain adopts a right-handed staple conformation, which is identical to that of naturally occurring disulfides spanning adjacent antiparallel β-strands (Harrison and Sternberg, 1996). Due to the geometrical requirements of the disulfide, the distance separating the two C_α atoms is reduced by 0.8 Å relative to wtYFP, resulting in a local constriction of the two β-strands at the site of the disulfide bridge (Figure 5C). This is brought about mainly by a movement of Cys149 towards β-strand 10. Movement of Asn164, Phe165 and Lys166 (part of β-strand 8) in the opposite direction leads to an unzipping of the β-sheet between strands 7 and 8 and the concomitant loss of three

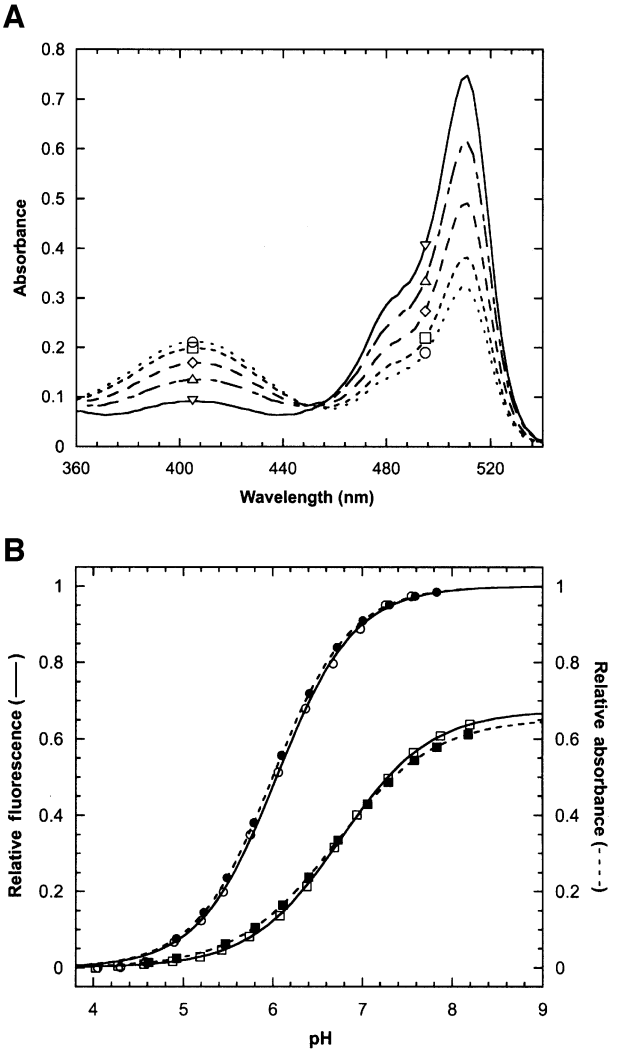

Fig. 4. Redox state-dependent spectral properties of rxYFP$^{149}_{202}$ at 30°C. (**A**) Absorption spectra were recorded after equilibration of the protein in redox buffers with [GSH]^2/[GSSG] ratios of 0.004 M (open circles), 0.55 M (open squares), 2.17 M (open diamonds) and 8.13 M (open triangles) (see Figure 3A). Reduced protein (open inverted triangles) was obtained by incubation with 10 mM DTT for 2 h. (**B**) The relative fluorescence (open symbols) and relative absorbance (closed symbols) of reduced (circles) and oxidized (squares) rxYFP$^{149}_{202}$ as a function of pH. Data were fitted as described in Materials and methods. The estimated values of the chromophore pK_a and the Hill coefficient (n) are given in the text.

main chain hydrogen bonds (one of them mediated by a water molecule; marked with dashed lines in Figure 5C). On the molecular surface, the strand separation is evident as a narrow, water-filled groove running along the β-strands. However, direct solvent access to the chromophore, which is located immediately behind the strands, is prevented due to steric blocking by the side chain of His148 (see below).

In wtYFP, the imidazole of His148 is wedged between strands 7 and 8 (Wachter *et al.*, 1998). It receives a hydrogen bond from the backbone of Arg168 and serves as an obligate hydrogen bond donor, via $N\delta_1$, to the phenolate oxygen of Tyr66 (Figures 5C and 6D). Site-directed mutagenesis of His148 has shown this interaction to be highly important in stabilizing the negatively charged deprotonated state of the chromophore (Elsliger *et al.*,

Table I. Data collection and refinement statistics

Data collection		Refinement	
Wavelength (Å)	1.0362	R_{conv} (%)	18.3
X-ray source	711 Lund	R_{free} (%)	21.2
Resolution (Å)		Resolution (Å)	78.09–1.50
overall	78.09–1.50	No. of reflections	
outer shell	1.55–1.50	Working set	109 885
No. of reflections		Test set	5546
overall	750 960	No. of atoms	
unique	116 321	Protein	5627
Mosaicity	0.25	Solvent	840
R_{sym} (%)		*B*-factor, protein atoms (Å^2)	16.8
overall	3.3	*B*-factor, solvent atoms (Å^2)	31.1
outer shell	43.9	R.m.s.d. bond distance (Å)	0.011
$I/\sigma I$		R.m.s.d. bond angle (°)	1.8
overall	18.3	Ramachandran plot, residues in	
outer shell	2.0	Most favourable regions (%)	90.8
Completeness (%)		Additional allowed regions (%)	9.0
overall	89.1	Disallowed regions (%)	0.0
outer shell	72.9	Estimated coordinate error from sigmea (Å)	0.16
		C–V estimated coordinate error from sigmea (Å)	0.16

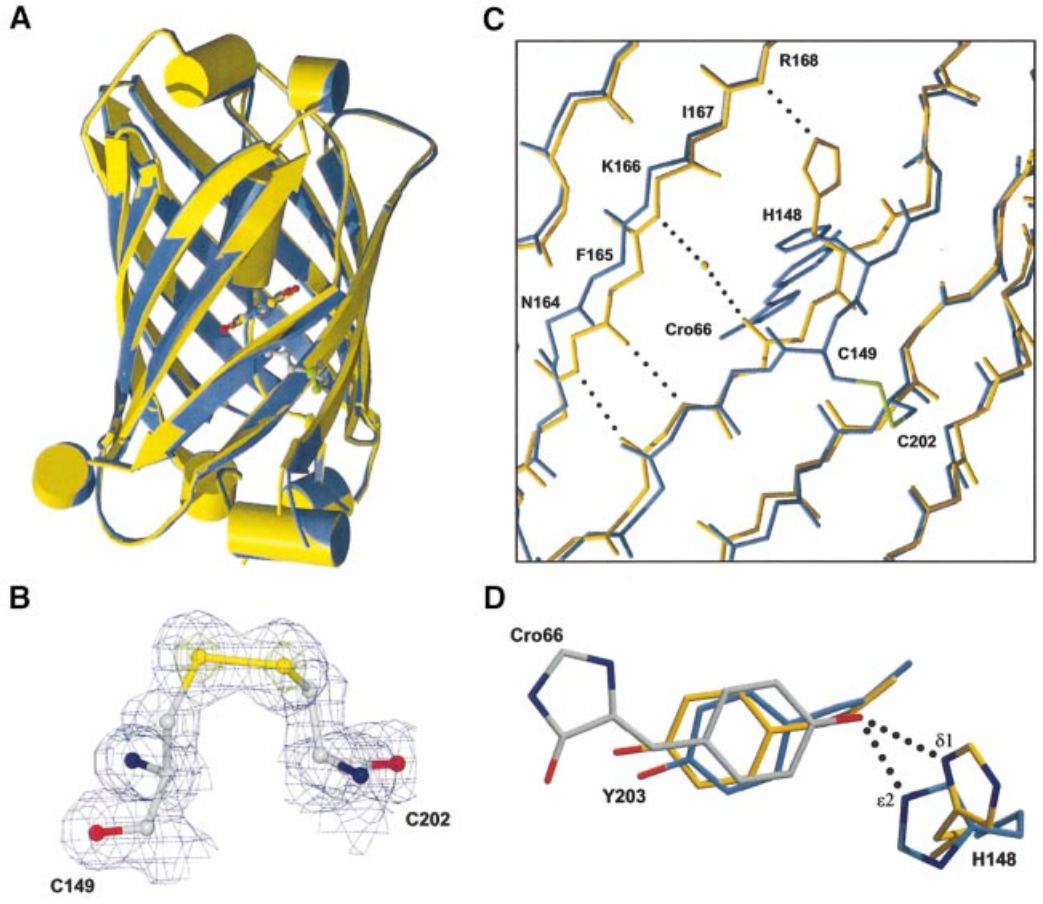

Fig. 5. Crystal structure of oxidized rxYFP$^{149}_{202}$. (**A**) Superposition of oxidized rxYFP$^{149}_{202}$ (throughout the figure in blue) and wtYFP (throughout in yellow; Wachter *et al*., 1998) (r.m.s. deviation is 0.5 Å for equivalent C_α atoms). The chromophore, Cys149 and Cys202 are shown as ball-and-stick representations with the disulfide bond coloured green. (**B**) The $2F_o - F_c$ electron density map of the C149–C202 disulfide bridge (contoured at 1σ in blue and at 8σ in green). Superimposed is the final model of the disulfide bridge, which adopts the right-handed staple conformation. (**C**) Overlay of the backbone trace of wtYFP and oxidized rxYFP$^{149}_{202}$. Also shown are the disulfide bond (in green), the side chain of His148 and the chromophore (Cro66). The dashed lines indicate those hydrogen bonds that are present in wtYFP but absent in the rxYFP$^{149}_{202}$ structure. (**D**) Position of Tyr203 and His148 relative to the chromophore. The superimposed chromophore structures of rxYFP$^{149}_{202}$ and wtYFP are shown in grey. Dashed lines indicate hydrogen bonds to the δ_1 and ε_2 nitrogens of His148.

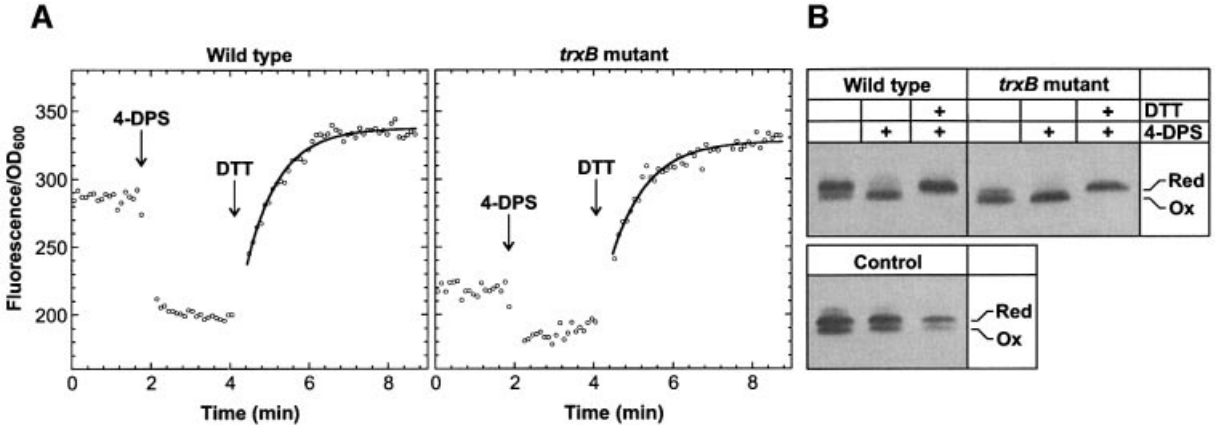

Fig. 6. Redox state of rxYFP$^{149}_{202}$ expressed in wild-type *E.coli* and a *trxB* mutant at 30°C. (**A**) Fluorescence was monitored continuously at 523 nm in a standard fluorimeter (see Materials and methods). From the initial fluorescence and the fluorescence after sequential addition of 50 µl of 3.6 mM 4-DPS and 50 µl of 1 M DTT to 900 µl of the cultures, the proportion of oxidized reporter in the two strains was calculated to 53% (wild type) and 86% (*trxB*), respectively. (**B**) Western blot detection of rxYFP$^{149}_{202}$ in the cultures before (lane 1) and after treatment with 4-DPS and DTT (lanes 2 and 3, respectively). In the lanes marked 'Control' were loaded equal amounts of reduced and oxidized rxYFP$^{149}_{202}$ at increasing dilution to show that the anti-GFP antibodies used bind with lower affinity to the oxidized reporter. Quantitative densitometric analysis of the bands corresponding to the untreated cultures, taking into account the weaker binding of the antibodies to the oxidized protein, indicated 50% oxidized reporter in the wild type and 83% in the *trxB* mutant.

1999). Substitution by glycine or glutamine residues, which do not hydrogen-bind to the chromophore, lowers the equilibrium constant for ionization by more than one order of magnitude (Wachter *et al*., 1998, 2000). In oxidized rxYFP$^{149}_{202}$, a major repositioning of His148 has taken place. Relative to wtYFP, it has moved away from the plane of the β-sheet by 1.4 Å and the imidazole side chain has rotated 108° around the χ_1 bond (Figure 5D). It is now in a position where it can interact with the chromophore phenolic oxygen through the Nε_2 atom. As the hydrogen bond partner to the Nδ_1 atom is a solvent molecule (located in the groove between the β-strands 7 and 8), Nε_2 can serve as both a donor and an acceptor of the hydrogen bond depending on the protonation state of Tyr66. The loss of directionality of the hydrogen bond is most likely to be the major cause of the observed increase in the chromophore pK_a.

In the interior of the protein, the chromophore has moved 0.7 Å away from the gap in the β-sheet and now occupies a position similar to that of wild-type GFP and S65T GFP (Ormo *et al*., 1996; Yang *et al*., 1996). The side chain of Tyr203 has rotated 30° around the χ_1 bond in the same direction. Compared with the off-centred parallel displaced arrangement of the Tyr203 side chain and the chromophore phenol in wtYFP, the two aromatic rings are positioned at skewed angles in rxYFP$^{149}_{202}$ (Figure 5D). It presently is not clear to what extent this misalignment or other small-scale movements of side chains in the immediate chromophore environment contribute to the observed drop in the molar extinction coefficient upon oxidation.

Redox monitoring in the cytoplasm

To demonstrate the functionality of rxYFP$^{149}_{202}$ *in vivo*, it was expressed in the cytoplasm of wild-type *E.coli* and an isogenic strain disrupted in the *trxB* gene encoding thioredoxin reductase. Deficiency of *trxB* leads to the accumulation of thioredoxin in the oxidized state, which promotes the incorporation of disulfide bonds into nascent cytoplasmic proteins (Derman *et al*., 1993; Stewart *et al*., 1998).

Fluorescence measurements were carried out in a standard fluorimeter after expression of the reporter from the *lac* promoter in exponentially growing cells for >10 generations. As expected, fluorescence intensity per OD_{600} was found to be highest for the wild type, indicating increased levels of oxidized rxYFP$^{149}_{202}$ in the *trxB* mutant (Figure 6A). Due to the dependency of fluorescence intensity on the protein concentration, calibration was required to determine the exact ratio between oxidized and reduced reporter. This was carried out by measuring the fluorescence after sequential addition of oxidant (F_{ox}) and reductant (F_{red}) directly to the culture in the cuvette. After addition of the membrane-permeable thiol-oxidant 4,4′-dithiodipyridine (4-DPS; Grassetti and Murray, 1967) and DTT, the fraction of oxidized reporter in the wild type and the *trxB* mutant was found to be 53 ± 3 and 86 ± 3%, respectively. Similar distributions were obtained by western blotting (Figure 6B). Oxidation of rxYFP$^{149}_{202}$ also occurred after addition of the widely used thiol-oxidant diamide although with a rate constant more than two orders of magnitude lower than that of oxidation by 4-DPS.

Based on the measured values of F_{red}/F_{ox} and the correlation between fluorescence and pH given in Figure 4B, the pH in the cytoplasmic compartment of the two strains could be estimated to 7.4 ± 0.1. This corresponds well with the value of 7.5 determined by ^{31}P NMR in aerobically respiring *E.coli* cells grown at neutral pH (Slonczewski *et al*., 1981). While oxidation of the reporter by 4-DPS was too fast (within the mixing time in the cuvette) to allow for a kinetic characterization of the reaction, reduction by DTT occurred over minutes. The progress curve conformed to pseudo first-order kinetics from which apparent second-order rate constants of 30 ± 1 M/min (wild type) and 28 ± 1 M/min (*trxB*

mutant) could be extracted. The elevated pH of the cytosol most probably accounts for the slightly higher values of k_2 as compared with those determined *in vitro* (see Figure 3B).

Discussion

Functional and structural properties of rxYFP$^{149}_{202}$

In an effort to visualize the formation of disulfide bonds in living cells, redox-active cysteines were introduced into YFP. Of the four double-cysteine mutants constructed, only rxYFP$^{149}_{202}$ exhibited a change in the intrinsic fluorescence sufficient to enable *in vivo* redox monitoring. The >2-fold change observed at neutral pH is comparable in magnitude with the dynamic range of other YFP-based reporters (Miyawaki *et al*., 1997; Jayaraman *et al*., 2000). However, due to differential pH sensitivities of the reduced and oxidized state, the dynamic range was found to vary substantially according to the pH. Thus, at pH 6.5, corresponding to the pH in the cytoplasm of yeast (Calahorra *et al*., 1998), the relative difference between the two redox states was 2.9 as compared with a factor of only 1.75 at pH 7.5 (the cytoplasm of *E.coli*).

Spectroscopic studies showed the oxidation-induced reduction of the intrinsic fluorescence to be caused by the combined effects of (i) a shift in the equilibrium between the two chromophore protonation states towards the non-fluorescent, protonated state and (ii) a lower molar extinction coefficient of the fluorescent, deprotonated chromophore. Quantum yield therefore appears to be unaffected by disulfide bond formation, implying that the disulfide bond itself does not quench the chromophore fluorescence. The crystal structure of oxidized rxYFP$^{149}_{202}$ rather points to a role for the disulfide bond as a source of strain, which through a distortion of the β-barrel perturbs the local environment of the chromophore. The importance of the exact position of the disulfide bond in bringing about this change is illustrated by the other two double-cysteine mutants, where fluorescence changes of only ~1.2-fold were observed, although the disulfide bond in these cases is <8 Å away from the 149–202 site. The location of the cysteine pair also had a dramatic effect on the redox potential. While the disulfide bond between Cys147 and Cys204 (K_{ox} = 2.4 M; data not shown) was almost as stable as that between Cys149 and Cys202, moving it to the 202–225 site resulted in a >10^4-fold decrease in the equilibrium constant (K_{ox}) with glutathione (data not shown). One of the major factors contributing to this large difference in stability is probably the lack of backbone hydrogen bonds between the cysteines in rxYFP$^{149}_{202}$ and rxYFP$^{147}_{204}$, which allows the two residues to approach each other relatively unhindered upon oxidation (in the right-handed staple conformation, the C_α interatomic distance is ~3.9 Å as compared with the normal distances of ~4.5 and ~5.5 Å between adjacent antiparallel β-strands; Wouters and Curmi, 1995). In rxYFP$^{202}_{225}$, on the other hand, two main chain hydrogen bonds have to be broken or at least distorted for the disulfide to adopt the right geometry. This is an energetically costly process, decreasing the stability of the disulfide. The unfavourable situation of having a disulfide bond bridging two backbone hydrogen-bonded cysteines is emphasized by the fact that disulfides spanning adjacent antiparallel β-strands in natural proteins occur exclusively at the so-called wide-pair hydrogen bonding positions (Harrison and Sternberg, 1996).

In vivo redox monitoring

In a screen for mutants that would allow a signal-sequenceless version of alkaline phosphatase to fold into its active, disulfide-bonded conformation, Derman *et al*. (1993) identified thioredoxin reductase (trxB) as being a key determinant of the cytoplasmic thiol–disulfide redox status. Using rxYFP$^{149}_{202}$ as an indicator of the cytoplasmic redox state, we reached the same result. Upon disruption of the *trxB* gene, the fraction of disulfide-bonded reporter increased by >30%, corresponding to a shift in the redox potential from –259 mV to –237 mV (calculated from the actual distribution of the reporter between the two redox states assuming a pH of 7.0). Interestingly, half of the reporter was already oxidized in the wild type. Only in very few cases have stable disulfide bonds been observed in cytosolic proteins (Nilsson *et al*., 1991; Locker and Griffiths, 1999). Based on the following observations, we believe the cytosolic pool of oxidized glutathione to be the primary oxidant of the reporter: (i) reduced thioredoxin (trxA) does not react with oxidized rxYFP$^{149}_{202}$ *in vitro* (data not shown); (ii) the cytoplasmic GSH/GSSG redox potential, roughly estimated to be within –220 to –245 mV [using GSH/GSSG ratios of 1:50–1:200 (Hwang *et al*., 1992; Tuggle and Fuchs, 1985) and a concentration of GSH of 3.6–6.6 mM (Kosower and Kosower, 1978)], is close to that determined using rxYFP$^{149}_{202}$, as would be expected if the two redox pairs were in equilibrium. It is presently not known whether increased amounts of oxidized glutathione are responsible for the higher proportion of oxidized rxYFP$^{149}_{202}$ in the *trxB* mutant or whether disulfide bond formation during folding catalysed by oxidized thioredoxin also plays a role. *In vitro* refolding of acid-denatured rxYFP$^{149}_{202}$ shows that the oxidized state folds as efficiently as the reduced state (data not shown).

Seen in a broader perspective, the above findings raise the question as to why cytoplasmic proteins are devoid of disulfide bonds. Clearly, sufficient oxidation potential is present for them to form. Moreover, disulfide bonds serving structural purposes are often more stable than that in rxYFP$^{149}_{202}$, making oxidation an even more favourable reaction (Gilbert, 1990). Part of the reason is probably that disulfide bond formation in the absence of a disulfide catalyst in most cases is too slow to compete with protein folding (Stewart *et al*., 1998). In rxYFP$^{149}_{202}$, however, the situation is quite different, as disulfide bond formation is not restricted to the short period of time it takes for the protein to fold but can also take place in the native protein.

In summary, by rational disulfide engineering on the YFP, we have created a non-invasive, redox-sensitive reporter and furthermore demonstrated its functionality *in vivo*. The ability to functionally express GFP in virtually any organism combined with its targetability to the different subcellular compartments should make it a highly useful redox reporter in a wide range of different applications. It is important to note that its use is not restricted to compartments that are normally reducing; redox monitoring in oxidizing environments such as the

periplasm and the endoplasmic reticulum should also be possible.

Materials and methods

Cloning and mutagenesis of YFP

Construction of the four YFP variants shown in Figure 1A was based on a synthetic, *E.coli* codon-optimized YFP gene present in the pFHC2191 plasmid (DDBJ/EMBL/GenBank accession No. AF325903). Relative to wild-type GFP, it contains the following mutations: S65A/V68L/S72A/Q80R/M153V/T203Y/D234H. Cysteines were introduced by PCR-based site-directed mutagenesis using standard methods. Cys48 was mutated to either alanine, methionine, threonine or valine by PCR using a degenerate oligonucleotide. The C48V mutation gave the brightest colonies at 37°C and was therefore incorporated into the YFP template. For overexpression of protein, the four mutant genes were transferred as *Nde*I–*Spe*I fragments to the *Nde*I–*Nhe*I site of the pET24 vector (Novagen) and finally introduced into the BL21(DE3) strain (Novagen).

Expression and purification

Cultures were grown at 37°C in terrific broth with 30 μg/ml kanamycin (Sambrook *et al*., 1989). At an OD_{600} of 2.5, the growth temperature was shifted to 22°C and protein expression induced by addition of isopropyl-β-D-thiogalactopyranoside (IPTG) to 0.25 mM. After 17 h of incubation, the cells were harvested, resuspended in 20 mM potassium phosphate buffer pH 7.5, 1 mM EDTA (3 ml/g wet pellet), and lysed by three freeze–thaw cycles. The lysate was cleared by centrifugation and subsequently loaded onto a DE52 (Whatman) anion exchange column. The protein was eluted with a linear gradient from 0 to 0.5 M NaCl in lysis buffer. Highly fluorescent fractions were pooled, adjusted to 20% saturation with ammonium sulfate, and applied to a phenyl-Sepharose (Amersham Pharmacia Biotech) column. The ammonium sulfate concentration was decreased linearly to 0%, and fluorescent fractions, which eluted at the end of the gradient, were pooled and dialysed overnight against 5 mM potassium phosphate pH 7.0. Finally, the protein was subjected to anion exchange chromatography on a Resource Q column (Amersham Pharmacia Biotech) equilibrated in 5 mM potassium phosphate pH 7.0. The protein eluted at ~0.1 M NaCl. Pooled fractions were dialysed against water and stored at –18°C. The protein is estimated to be >95% pure as judged by SDS–PAGE.

Crystallization and data collection

Oxidized $rxYFP^{149}_{202}$ was concentrated to 24 mg/ml in 10 mM HEPES pH 8.0 using a Centriprep-10 concentrator (Amicon). Crystallization was performed by the hanging drop vapour diffusion method. Equal volumes (2 μl) of protein solution and mother liquor, containing 100 mM HEPES pH 8.0, 100 mM $MgCl_2$ and 14% (w/v) PEG4000 (Merck), were mixed in a single droplet and equilibrated against 1 ml of mother liquor. Rectangular-shaped crystals with approximate dimensions of $0.5 \times 0.1 \times 0.1$ mm^3 appeared within 4–5 days at 22°C. Before data collection, the crystals were transferred to mother liquor containing 30% glycerol as cryoprotectant and subsequently flash frozen in liquid nitrogen. Diffraction data were collected at beamline 711 at MAX-Lab, Lund University. The data extended to 1.5 Å (Table I). They were integrated and scaled using the HKL software package (Otwinowski and Minor, 1997).

Structure determination

The crystals of oxidized $rxYFP^{149}_{202}$ contain three molecules per asymmetric unit. Initial phases were determined by molecular replacement (Navaza and Saludjian, 1997) with wtYFP (Wachter *et al*., 1998) as a search model. The models were refined by slow-cool annealing (Brünger *et al*., 1998), first applying strict non-crystallographic symmetry (NCS) to the molecules and in later stages with no NCS imposed. Individual and restrained *B*-factors were used in the final cycles of the refinement. The final *B*-factors of the sulfurs in the disulfide bridge ($<B_S\gamma>$ = 13.1 $Å^2$) resemble the *B*-factors of its immediate environment. An attempt to refine the occupancy of the sulfur atoms in the disulfide bridge resulted in occupancies of 1.00 ± 0.02, and therefore they were assigned a fixed value of 1.00. The final model consists of three monomers of 230 residues each (residues 2–231), two chloride ions and 840 water molecules. The positional differences between the NCS-related molecules are located primarily in four loops participating in intermolecular interactions. No significant differences are found in the chromophore environment. Refinement statistics are given in Table I. Significant $2F_o - F_c$ and $F_o - F_c$ electron density is observed in all three molecules close to Cys70. The excess electron density has a centre 1.5 Å from the Sγ position, indicating that the cysteine is in an oxidized state. An oxygen atom at this position is not included in the model, as the exact oxidation state of Cys70 is not known.

Figures were generated using MOLSCRIPT (Kraulis, 1991), Raster3D (Merritt and Bacon, 1997) and Dino (http://www.dino3d.org). The refined coordinates and structure factors of oxidized $rxYFP^{149}_{202}$ have been deposited in the Protein Data Bank, accession code 1h6r.

Protein techniques

Thiol concentrations were determined using Ellman's reagent (Riddles *et al*., 1979). GSSG in stock solutions was quantified by absorption at 248 nm (ε = 382 M/cm; Chau and Nelson, 1991). Fluorescence measurements were performed using a Perkin-Elmer Luminescence Spectrometer LS50B with a thermostatted, stirred single-cell holder. Unless stated otherwise, excitation and emission wavelengths were 512 and 523 nm, respectively, at 3 nm slit widths. Absorption spectra were measured using a thermostatted Perkin-Elmer UV/VIS λ16 Spectrometer.

Determination of redox potential

Redox potentials of the YFP variants were determined from their reaction with glutathione essentially as described elsewhere (Loferer *et al*., 1995). Oxidized protein (~0.3 μM) was incubated in 100 mM potassium phosphate pH 7.0, 1 mM EDTA (thoroughly purged with argon) containing varying concentrations of oxidized (5–50 μM) and reduced glutathione (250 μM–225 mM). After equilibration of the protein samples under an argon atmosphere for 21 h at 30°C, the redox state of the protein was assessed by spectrofluorimetry. In order to compensate for air oxidation of GSH, an aliquot of the reaction mixture was quenched by addition of formic acid to 10% (v/v) and the equilibrium concentration of GSSG determined by HPLC as described below. The equilibrium constant, K_{ox}, was determined by fitting the data to $F = F_{ox} + (F_{red} - F_{ox})([GSH]^2/[GSSG])/(K_{ox}+[GSH]^2/[GSSG])$, where F_{red} and F_{ox} are the fluorescence of the reduced and oxidized protein, respectively.

To determine the concentration of GSSG, 100 μl of the quenched samples were loaded onto a C_{18} reversed phase column (Vydac 218TP5415). GSSG was eluted with a linear gradient (0–5% in 12 min; 1 ml/min) of acetonitrile in 0.1% (v/v) trifluoroacetic acid and detected by absorption at 248 nm. The concentration of GSSG was determined by relating the integrated peak area to a GSSG standard curve. Linearity was observed in the range from 2 to 60 nmol.

pH titrations

pH titrations of reduced and oxidized $rxYFP^{149}_{202}$ were carried out at 30°C in solutions containing 100 mM K_2SO_4 and 25 mM of one of the following buffers: citrate pH 4.0–5.2, MES pH 5.5–7.0, HEPES pH 7.0–8.0 or Bicine pH 8.2–8.8. Buffers were chosen so that they did not contain any halides or other ions known to quench the YFP fluorescence (Jayaraman *et al*., 2000). The protein was diluted 50-fold into buffer and, after 5 min of equilibration, fluorescence intensity at 523 nm or absorbance at 512 nm was recorded. The apparent pK_a of the chromophore was obtained by fitting the data to $S = S_{max}/[1 + 10^{n(pKa - pH)}]$, where S_{max} is the limiting fluorescence/absorbance at high pH and *n* is the Hill coefficient.

In vivo characterization of rxYFP

The gene encoding $rxYFP^{149}_{202}$ was excised from the pFHC2191 vector and inserted as an *Nde*I fragment into the corresponding site of pFHC2102 (F.G.Hansen, unpublished), a pBR322-derived (Bolivar *et al*., 1977) expression vector carrying the IPTG-inducible *lacP*(A1/04/03) promotor and the wild-type *lacI* gene from pBEX5BA (Diederich *et al*., 1994). The resulting plasmid, pHOJ124, was introduced into the *E.coli* strain MC1000 [*ara*D139Δ(*ara-leu*)7697Δ*lac*X-74 *gal*U *gal*K *str*A] and HOJ156. The latter was constructed by transducing the *trxB*::*kan* mutation present in AD494 (Novagen; Derman *et al*., 1993) into MC1000 by P1 transduction.

The strains were grown at 30°C in AB minimal medium pH 7.0 (Clark and Maaløe, 1967) supplemented with 1 μg/ml thiamine, 100 μg/ml ampicillin, 0.2% glucose and all the 20 amino acids except cysteine at 50 μg/ml. To ensure identical and reproducible levels of protein expression, log-phase cultures (OD_{600} <0.5) were maintained for at least 10 generations in the presence of 1 mM IPTG before fluorescence measurements were performed. At an OD_{600} of 0.4–0.5, 900 μl of the culture were transferred to a pre-warmed cuvette. Fluorescence was monitored continuously at 523 nm, with excitation at 512 nm and slit

widths of 4 nm. After a stable baseline was obtained (F_{init}), 50 µl of 3.6 mM 4-DPS (in water; Aldrich) were added, followed by 50 µl of 1 M DTT (in water; Sigma) to oxidize (F_{ox}) and reduce (F_{red}), respectively, the protein. The oxidant, 4-DPS, as well as its reaction product 4-thiopyridone absorb well below 400 nm and thus do not interfere with the fluorescence measurements (Grassetti and Murray, 1967). The fraction of oxidized reporter in the untreated culture was calculated from the expression: $1 - (F_{init} - F_{ox})/(F_{red} - F_{ox})$.

The redox state of $rxYFP^{149}_{202}$ was also determined by western blotting. A 1 ml aliquot of culture (before or after treatment with 4-DPS or DTT) was acid quenched by addition of 1/10 volume of 100% (w/v) trichloroacetic acid. After centrifugation, the pellet was washed twice with 0.5 ml of ice-cold acetone and then resuspended in 200 µl of 2% SDS, 100 mM Tris–HCl pH 8.0, 40 mM *N*-ethylmaleimide (Sigma). Following 1 h of incubation at room temperature, the sample was separated on a 12% SDS–polyacrylamide gel, blotted to a nitrocellulose membrane (Hybond-C extra; Amersham Life Sciences) and probed with rabbit polyclonal anti-GFP antibodies (IgG fraction; Molecular Probes). The primary antibodies were detected using horseradish peroxidase-conjugated swine anti-rabbit antibodies (DAKO-immunoglobulins A/S) and the enhanced chemiluminescence western blot detection kit (ECL+; Amersham Pharmacia Biotech).

Acknowledgements

We thank Anette W.Bruun and Søs Koefoed for excellent technical assistance, Morten Kielland-Brandt and Kresten Lindorff-Larsen for critically reading the manuscript, and Per Nørgaard for stimulating discussions. MAX-Lab, beamline 711 and Yngve Cerenius are also gratefully acknowledged. This work was supported by a grant from the Carlsberg Foundation to F.G.H. and by the European Community—Access to Research Infrastructure action of the Improving Human Potential Programme.

References

Aberg,A., Hahne,S., Karlsson,M., Larsson,A., Ormo,M., Ahgren,A. and Sjoberg,B.M. (1989) Evidence for two different classes of redox-active cysteines in ribonucleotide reductase of *Escherichia coli*. *J. Biol. Chem.*, **264**, 12249–12252.

Aslund,F. and Beckwith,J. (1999) The thioredoxin superfamily: redundancy, specificity and gray-area genomics. *J. Bacteriol.*, **181**, 1375–1379.

Baird,G.S., Zacharias,D.A. and Tsien,R.Y. (1999) Circular permutation and receptor insertion within green fluorescent proteins. *Proc. Natl Acad. Sci. USA*, **96**, 11241–11246.

Bardwell,J.C., McGovern,K. and Beckwith,J. (1991) Identification of a protein required for disulfide bond formation *in vivo*. *Cell*, **67**, 581–589.

Bolivar,F., Rodriguez,R.L., Greene,P.J., Betlach,M.C., Heyneker,H.L. and Boyer,H.W. (1977) Construction and characterization of new cloning vehicles. II. A multipurpose cloning system. *Gene*, **2**, 95–113.

Brejc,K., Sixma,T.K, Kitts,P.A., Kain,S.R., Tsien,R.Y., Ormo,M. and Remington,S.J. (1997) Structural basis for dual excitation and photoisomerization of the *Aequorea victoria* green fluorescent protein. *Proc. Natl Acad. Sci. USA*, **94**, 2306–2311.

Brünger,A.T. *et al*. (1998) Crystallography and NMR system: a new software suite for macromolecular structure determination. *Acta Crystallogr. D*, **54**, 905–921.

Calahorra,M., Martinez,G.A., Hernandez-Cruz,A. and Pena,A. (1998) Influence of monovalent cations on yeast cytoplasmic and vacuolar pH. *Yeast*, **14**, 501–515.

Casey,J.L., Coley,A.M., Tilley,L.M. and Foley,M. (2000) Green fluorescent antibodies: novel *in vitro* tools. *Protein Eng.*, **13**, 445–452.

Chattoraj,M., King,B.A., Bublitz,G.U. and Boxer,S.G. (1996) Ultra-fast excited state dynamics in green fluorescent protein: multiple states and proton transfer. *Proc. Natl Acad. Sci. USA*, **93**, 8362–8367.

Chau,M.H. and Nelson,J.W. (1991) Direct measurement of the equilibrium between glutathione and dithiothreitol by high performance liquid chromatography. *FEBS Lett.*, **291**, 296–298.

Clark,D.J. and Maaløe,O. (1967) DNA replication and the division cycle in *Escherichia coli*. *J. Mol. Biol.*, **23**, 99–112.

Cody,C.W., Prasher,D.C., Westler,W.M., Prendergast,F.G. and Ward,W.W. (1993) Chemical structure of the hexapeptide chromophore of the *Aequorea* green fluorescent protein. *Biochemistry*, **32**, 1212–1218.

Debarbieux,L. and Beckwith,J. (1999) Electron avenue: pathways of disulfide bond formation and isomerization. *Cell*, **99**, 117–119.

De Giorgi,F. *et al*. (1999) Targeting GFP to organelles. *Methods Cell Biol.*, **58**, 75–85.

Derman,A.I., Prinz,W.A., Belin,D. and Beckwith,J. (1993) Mutations that allow disulfide bond formation in the cytoplasm of *Escherichia coli*. *Science*, **262**, 1744–1747.

Diederich,L., Roth,A., Messer,W. (1994) A versatile plasmid vector system for the regulated expression of genes in *Escherichia coli*. *Biotechniques*, **16**, 916–923.

Elsliger,M.A., Wachter,R.M., Hanson,G.T., Kallio,K. and Remington,S.J. (1999) Structural and spectral response of green fluorescent protein variants to changes in pH. *Biochemistry*, **38**, 5296–5301.

Gilbert,H.F. (1990) Molecular and cellular aspects of thiol–disulfide exchange. *Adv. Enzymol. Relat. Areas Mol. Biol.*, **63**, 69–172.

Gilbert,H.F. (1995) Thiol/disulfide exchange equilibria and disulfide bond stability. *Methods Enzymol.*, **251**, 8–28.

Grassetti,D.R. and Murray,J.F.,Jr (1967) Determination of sulfhydryl groups with 2,2′- or 4,4′-dithiodipyridine. *Arch. Biochem. Biophys.*, **119**, 41–49.

Harrison,P.M. and Sternberg,M.J. (1996) The disulphide β-cross: from cystine geometry and clustering to classification of small disulphide-rich protein folds. *J. Mol. Biol.*, **264**, 603–623.

Heim,R., Prasher,D.C. and Tsien,R.Y. (1994) Wavelength mutations and posttranslational autoxidation of green fluorescent protein. *Proc. Natl Acad. Sci. USA*, **91**, 12501–12504.

Holmgren,A. (1989) Thioredoxin and glutaredoxin systems. *J. Biol. Chem.*, **264**, 13963–13966.

Huber-Wunderlich,M. and Glockshuber,R. (1998) A single dipeptide sequence modulates the redox properties of a whole enzyme family. *Fold. Des.*, **3**, 161–171.

Hwang,C., Sinskey,A.J. and Lodish,H.F. (1992) Oxidized redox state of glutathione in the endoplasmic reticulum. *Science*, **257**, 1496–1502.

Inouye,S. and Tsuji,F.I. (1994) Evidence for redox forms of the *Aequorea* green fluorescent protein. *FEBS Lett.*, **351**, 211–214.

Jakob,U., Muse,W., Eser,M. and Bardwell,J.C. (1999) Chaperone activity with a redox switch. *Cell*, **96**, 341–352.

Jayaraman,S., Haggie,P., Wachter,R.M., Remington,S.J. and Verkman,A.S. (2000) Mechanism and cellular applications of a green fluorescent protein-based halide sensor. *J. Biol. Chem.*, **275**, 6047–6050.

Jonda,S., Huber-Wunderlich,M., Glockshuber,R. and Mossner,E. (1999) Complementation of DsbA deficiency with secreted thioredoxin variants reveals the crucial role of an efficient dithiol oxidant for catalyzed protein folding in the bacterial periplasm. *EMBO J.*, **18**, 3271–3281.

Kosower,N.S. and Kosower,E.M. (1978) The glutathione status of cells. *Int. Rev. Cytol.*, **54**, 109–160.

Kraulis,P. (1991) MOLSCRIPT: a program to produce both detailed and schematic plots of proteins. *J. Appl. Crystallogr.*, **24**, 946–950.

Krause,G., Lundstrom,J., Barea,J.L., Pueyo,D.L.C. and Holmgren,A. (1991) Mimicking the active site of protein disulfide-isomerase by substitution of proline 34 in *Escherichia coli* thioredoxin. *J. Biol. Chem.*, **266**, 9494–9500.

Lin,T.Y. and Kim,P.S. (1989) Urea dependence of thiol–disulfide equilibria in thioredoxin: confirmation of the linkage relationship and a sensitive assay for structure. *Biochemistry*, **28**, 5282–5287.

Locker,J.K. and Griffiths,G. (1999) An unconventional role for cytoplasmic disulfide bonds in vaccinia virus proteins. *J. Cell Biol.*, **144**, 267–279.

Loferer,H., Wunderlich,M., Hennecke,H. and Glockshuber,R. (1995) A bacterial thioredoxin-like protein that is exposed to the periplasm has redox properties comparable with those of cytoplasmic thioredoxins. *J. Biol. Chem.*, **270**, 26178–26183.

Martin,J.L. (1995) Thioredoxin—a fold for all reasons. *Structure*, **3**, 245–250.

Merritt,E.A. and Bacon,D.J. (1997) Raster3D: photorealistic molecular graphics. *Methods Enzymol.*, **277**, 505–524.

Miyawaki,A., Llopis,J., Heim,R., McCaffery,J.M., Adams,J.A., Ikura,M. and Tsien,R.Y. (1997) Fluorescent indicators for Ca^{2+} based on green fluorescent proteins and calmodulin. *Nature*, **388**, 882–887.

Navaza,J. and Saludjian,P. (1997) AMoRe: an automated molecular replacement program package. *Methods Enzymol.*, **276**, 581–594.

Nilsson,B., Berman-Marks,C., Kuntz,I.D. and Anderson,S. (1991)

Secretion incompetence of bovine pancreatic trypsin inhibitor expressed in *Escherichia coli*. *J. Biol. Chem.*, **266**, 2970–2977.
Niwa,H., Inouye,S., Hirano,T., Matsuno,T., Kojima,S., Kubota,M., Ohashi,M. and Tsuji,F.I. (1996) Chemical nature of the light emitter of the *Aequorea* green fluorescent protein. *Proc. Natl Acad. Sci. USA*, **93**, 13617–13622.
Ormo,M., Cubitt,A.B., Kallio,K., Gross,L.A., Tsien,R.Y. and Remington,S.J. (1996) Crystal structure of the *Aequorea victoria* green fluorescent protein. *Science*, **273**, 1392–1395.
Otwinowski,Z. and Minor,W. (1997) Processing of X-ray diffraction data collected in oscillation mode. *Methods Enzymol.*, **276**, 307–326.
Palm,G.J. and Wlodawer,A. (1999) Spectral variants of green fluorescent protein. *Methods Enzymol.*, **302**, 378–394.
Prinz,W.A., Aslund,F., Holmgren,A. and Beckwith,J. (1997) The role of the thioredoxin and glutaredoxin pathways in reducing protein disulfide bonds in the *Escherichia coli* cytoplasm. *J. Biol. Chem.*, **272**, 15661–15667.
Reid,B.G. and Flynn,G.C. (1997) Chromophore formation in green fluorescent protein. *Biochemistry*, **36**, 6786–6791.
Remington,S.J. (2000) Structural basis for understanding spectral variations in green fluorescent protein. *Methods Enzymol.*, **305**, 196–211.
Riddles,P.W., Blakeley,R.L. and Zerner,B. (1979) Ellman's reagent: 5,5′-dithiobis(2-nitrobenzoic acid)—a reexamination. *Anal. Biochem.*, **94**, 75–81.
Rietsch,A. and Beckwith,J. (1998) The genetics of disulfide bond metabolism. *Annu. Rev. Genet.*, **32**, 163–184.
Rost,J. and Rapoport,S. (1964) Reduction-potential of glutathione. *Nature*, **201**, 185.
Sambrook,J., Fritsch,E.F. and Maniatis,T. (1989) *Molecular Cloning: A Laboratory Manual*, 2nd edn. Cold Spring Harbor Laboratory Press, Cold Spring Harbor, NY.
Slonczewski,J.L., Rosen,B.P., Alger,J.R. and Macnab,R.M. (1981) pH homeostasis in *Escherichia coli*: measurement by ^{31}P nuclear magnetic resonance of methylphosphonate and phosphate. *Proc. Natl Acad. Sci. USA*, **78**, 6271–6275.
Stewart,E.J., Aslund,F. and Beckwith,J. (1998) Disulfide bond formation in the *Escherichia coli* cytoplasm: an *in vivo* role reversal for the thioredoxins. *EMBO J.*, **17**, 5543–5550.
Szajewski,R.P. and Whitesides,G.M. (1980) Rate constants and equilibrium constants for thiol–disulfide interchange reactions involving oxidized glutathione. *J. Am. Chem. Soc.*, **102**, 2011–2026.
Topell,S., Hennecke,J. and Glockshuber,R. (1999) Circularly permuted variants of the green fluorescent protein. *FEBS Lett.*, **457**, 283–289.
Tsien,R.Y. (1998) The green fluorescent protein. *Annu. Rev. Biochem.*, **67**, 509–544.
Tuggle,C.K. and Fuchs,J.A. (1985) Glutathione reductase is not required for maintenance of reduced glutathione in *Escherichia coli* K-12. *J. Bacteriol.*, **162**, 448–450.
Wachter,R.M., Elsliger,M.A., Kallio,K., Hanson,G.T. and Remington,S.J. (1998) Structural basis of spectral shifts in the yellow-emission variants of green fluorescent protein. *Structure*, **6**, 1267–1277.
Wachter,R.M., Yarbrough,D., Kallio,K. and Remington,S.J. (2000) Crystallographic and energetic analysis of binding of selected anions to the yellow variants of green fluorescent protein. *J. Mol. Biol.*, **301**, 157–171.
Wouters,M.A. and Curmi,P.M. (1995) An analysis of side chain interactions and pair correlations within antiparallel β-sheets: the differences between backbone hydrogen-bonded and non-hydrogen-bonded residue pairs. *Proteins*, **22**, 119–131.
Wunderlich,M. and Glockshuber,R. (1993) Redox properties of protein disulfide isomerase (DsbA) from *Escherichia coli*. *Protein Sci.*, **2**, 717–726.
Yang,F., Moss,L.G. and Phillips,G.N.,Jr (1996) The molecular structure of green fluorescent protein. *Nature Biotechnol.*, **14**, 1246–1251.
Zheng,M., Aslund,F. and Storz,G. (1998) Activation of the OxyR transcription factor by reversible disulfide bond formation. *Science*, **279**, 1718–1721.

Received June 25, 2001; revised September 4, 2001; accepted September 7, 2001